Supporting file

Pulse Laser Induced Size-controllable and Symmetrical Ordering of Single Crystal Si Islands
Si Islands

*Dongfeng Qi [*a b c] Shiwei Tang [a] Letian Wang [b] Shixun Dai [a] Xiang Shen [a] Chen Wang[d] and Songyan Chen [c]*

[(a)] Laboratory of Infrared Materials and Devices,
The Research Institute of Advanced Technologies,
Ningbo University, Ningbo, Zhejiang, 315211, China

[(b)] Laser Thermal Laboratory
Department of Mechanical Engineering
University of California, Berkeley
Berkeley, CA 94720-1740, USA

[(c)] Semiconductor Photonics Research Center
Department of Physics
Xiamen University
Xiamen, 361005, People's Republic of China

[(d)] Fujian Provincial Key Laboratory of Optoelectronic Technology and Devices,
School of Optoelectronic and Communication Engineering,
Xiamen University of Technology, Xiamen, Fujian 361024, China

*Corresponding author. Tel.: +86 17858930656. Ningbo University, Ningbo, Zhejiang, 315211, China. E-mail: qidongfeng@nbu.edu.cn; sychen@xmu.edu.cn

Keywords
Pulse Laser Induced Size-controllable and Symmetrical Ordering of Single Crystal Si Islands

Patterned Si Nanofabrication Process.

Thermal resist layer was spin coated on the Si surface, and nanopatterned thermal resist stamps were prepared by casting mixed solutions of monomer (acrylamide, Acr) and crosslinker (bis) on soft mold (IPS@, one kind of special polymer produced by Obducat Technologies, Sweden). The IPS mold used here was replicated from hard nickel mold with nanoimprint machine (Obducat Eitire 6, Obducat Technologies Co., Sweden). After curing, the thermal resist stamps mold was peeled off from the soft IPS mold, and then soaked in 0.1 mol/L NaCl solution overnight. Prior to use, the stamps were dried on filter paper for 10 min and under a stream of N_2 for 10 s.

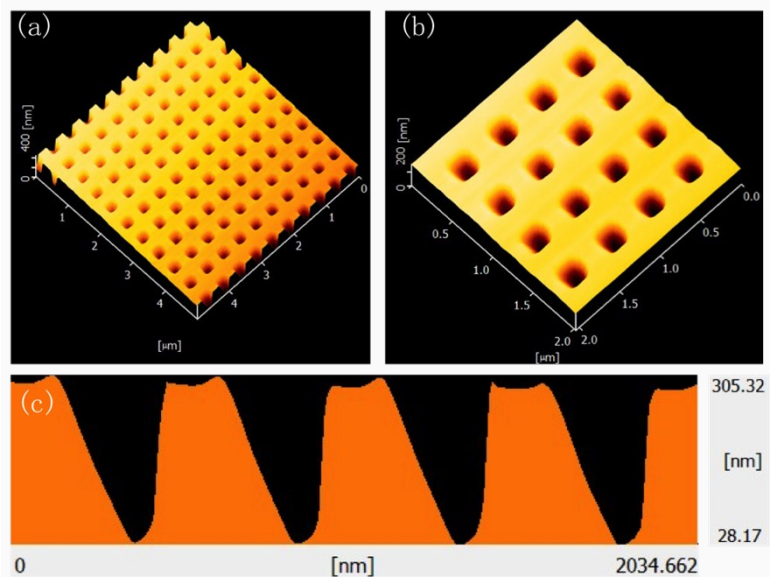

Figure 1. Intermediate polymer sheet with circular post patterns is used as a mask to fabricate circular holes on Si substrate. (a, b) are surface AFM images of patterned thermal resist layer; (c) is AFM images of height scans thermal resist nanowell.

After we got the patterned nanoholes on the thermal resist layer, next, Si wafer was subsequently etched to be a nanohole template with different size trenches. Thermal resist layer dry etch removal was performed with an Alcatel AMS200 in RIE mode using various SF_6 and C_4F_8 mixtures at a pressure of 10 mTorr at 20 ℃ in the RIE mode, and the fabricated Si nanoholes were passivated with a fluorinated polymer thin film via plasma polymerization of octafluorocyclobutane (C_4F_8) in the RIE system operating with the etching cycle. The C_4F_8

flow rate was 50 sccm, and the SF_6 flow rates were 30 sccm. Nanoholes with different diameter and depth can be fabricated after different etching time.

Laser processing setup.

And the nanosecond pulsed laser, which ran at a central wavelength of 248 nm with pulse duration of 25 ns and a repetition rate of 5 Hz, was used to perform nanosecond (ns) ablation experiments. The detailed information was set up as shown in figure S2(a). The KrF laser pulses of 248 nm wavelength and 25 ns temporal width impinged on silicon film targets. The laser beam was focused by a 5× infinity corrected, non-achromatic long working distance objective lens at normal incidence. A white illuminator was employed as an illumination source to provide real time images. These images were captured by a charge coupled device (CCD) camera via a 5× infinity objective lens. The oscilloscope was used to record the actual duration time of the processing laser signal. To ensure true representation, at least four images were examined at each fluences. Due to the limitation of the optical image, we cannot capture the detail islands information from the CCD images, as shown in the setup. But basing on the setup, we can see the start-time of the laser-induced island structures, and the detailed surface structures are captured by SEM images.

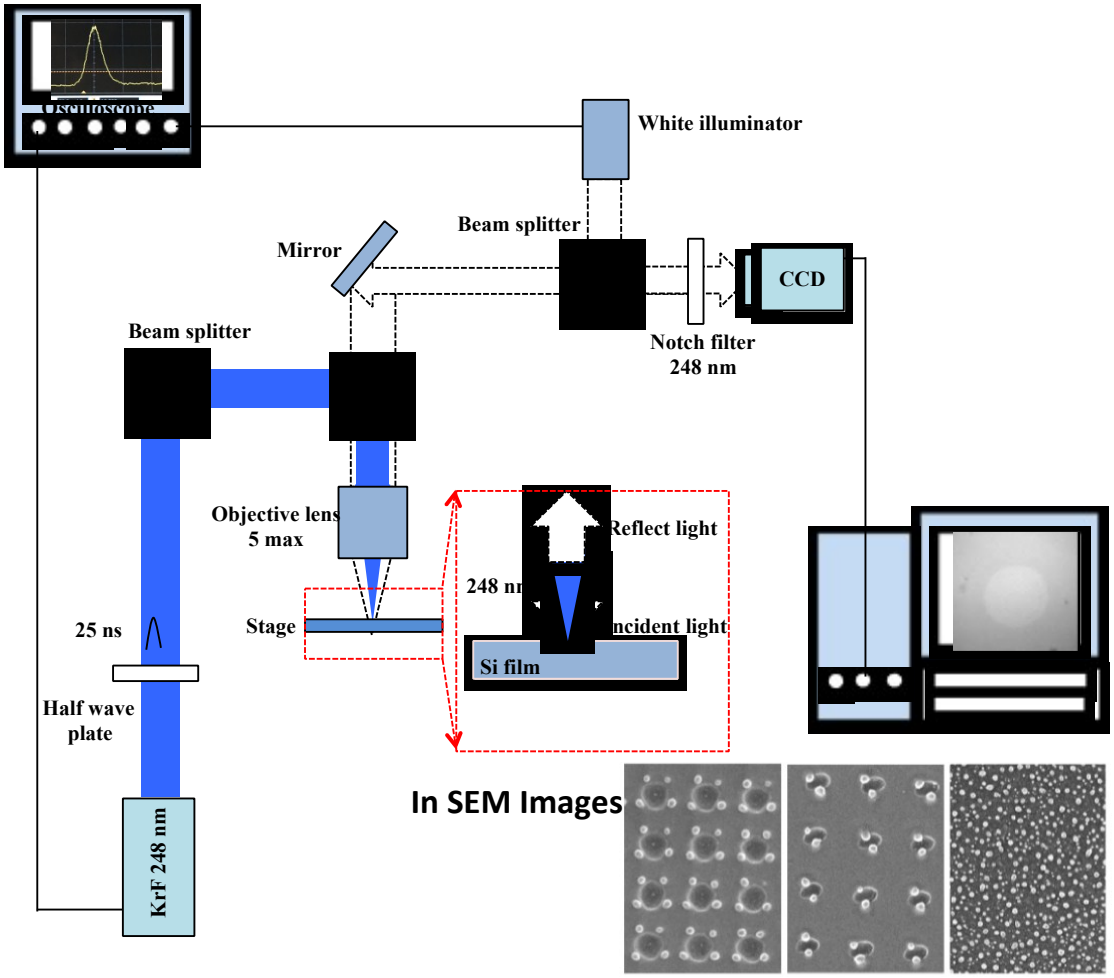

Figure 2. The setup of the laser induced periodic Si islands by an excimer laser pulse with 25ns duration

Surface morphology analyzes.

The morphologies of the formed surface structures were characterized by a scanning electron microscopy system (SEM, LEO 1530, with an operating voltage of 20 kV). The depth and diameter of the naoholes can be analyzed by atomic force microscopy (AFM) using Seiku Instruments SPI4000/SPA-400 system operating in tapping mode.

Theory simulation.

1.Melting depth calculation

During the laser annealing processes, we can assume that the photon energy is locally and instantaneously converted into heat because of the fast electron-photon energy transfer. When irradiating germanium with laser light at a sufficient energy density, a melted zone is formed in the material. As the pulse is highly monoenergetic, the melted zone is well defined and a sharp transition between the liquid and solid phase is formed. Moreover, we can assume that the irradiative heat loss at the surface is negligible and that the beam diameter is larger than the absorption length (about 5 nm at wavelength equal to 248 nm). Assuming that the lateral heat diffusion can be neglected, the process is described by the one-dimensional heat diffusion differential equation as follows:

$$\boldsymbol{C(T)}\rho\frac{\partial \boldsymbol{T}}{\partial \boldsymbol{t}} = \alpha(\boldsymbol{1}-\boldsymbol{R})\boldsymbol{I_0(t)}\exp^{-\alpha x} + \frac{\partial}{\partial \boldsymbol{x}}\left(\boldsymbol{K(T)}\frac{\partial \boldsymbol{T}}{\partial \boldsymbol{x}}\right), \tag{1}$$

where, ρ is the density, *C(T)* is the specific heat, α is the absorption coefficient here supposed dependent on the wavelength only, *K(T)* is the thermal conductivity, $I_0(t)$ is the Gaussian laser pulse having a FWHM duration time (25 ns), *R* is the reflectivity, and *T=T(x t)* is the temperature. The initial condition is $T(x,0)=T_0$, which represents the substrate temperature before the irradiation. The boundary condition:

$$\boldsymbol{K_s}\left.\frac{\partial \boldsymbol{T}}{\partial \boldsymbol{x}}\right|_{x_B} - \boldsymbol{K_l}\left.\frac{\partial \boldsymbol{T}}{\partial \boldsymbol{x}}\right|_{x_B} = \boldsymbol{L}\frac{\boldsymbol{dx_B}}{\boldsymbol{dt}}, \tag{2}$$

$$\boldsymbol{x}=\boldsymbol{0}, \frac{\partial \boldsymbol{T}}{\partial \boldsymbol{x}} = \boldsymbol{0}, \tag{3}$$

$$\boldsymbol{x}\to\infty, \boldsymbol{T}=\boldsymbol{T_0}, \tag{4}$$

In Eq. (2)-(4), j is either s for solid state or l for liquid state, L is the latent heat of melting, and x_B is the liquid-solid interface position. The Eq. (2) represents the heat transportation when germanium material changes from solid phase into the liquid phase. From the Eq. (3), we consider that the irradiative heat loss at the surface can be neglected. The thermodynamical and optical data used in the heat flow calculation come from the references. From the heat flow calculation, several parameters such as the depth of the molten layer, the melting duration and surface temperature of the samples can be evaluated as a function of laser fluence. The thermodynamical and optical data used in the heat flow calculation come from the references [1]-[4], as shown in Table I.

Table I

Table I Parameters for crystal Si (c-Si) used in heat calculation [1]-[4]

	c-Si
Melting point(K)	1688
R: reflection coefficient	0.57
α: absorption coefficient(cm^{-1})	2×10^{6}
ρ: density(g/cm^3)	2.33
L: latent heat(J/g)	1801
C: specific heat capacity(J/g·K)	C_s=0.864+8.36×10^{-5}×T−1.63×T^{-2} C_l=0.98
K: thermal conductivity(W/cm·K)	$K(T) = 1521\times T^{-1.226}$, 300K<T<1200K $K(T) = 8.96\times T^{-0.502}$, 1200K<T<1683K K_l=0.18

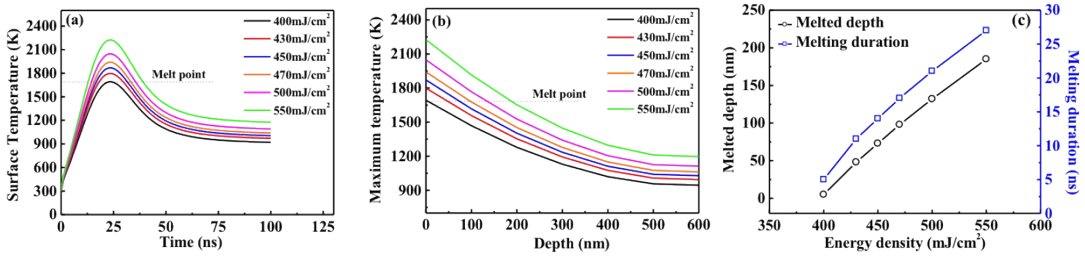

Figure 3. (a) Simulated surface temperature as a function of time for the applied laser fluences (b) Simulated maximum temperature reached as a function of depth for the applied laser fluences. The energy density used for simulation is form 400 to 550 mJ/cm^2. (c) Simulated melted depth and melting duration as a function of depth for the applied laser fluences. The energy densities used for simulation are form 400 to 550 mJ/cm^2.

2. The testing method for density and diameters of surface islands

For the method of calculating the density of the island structure, we firstly modified the SEM images, as shown below, in high contrast, and then, we count the islands in the square (400∗400 nm^2). Basing on the island counts in the square, we can generally get the islands density. Although this method maybe not quite exactitude，we selected at least four square to ensure true representation at each laser fluence. Figure S8 below shows surface morphology of Si islands irradiated of different laser fluences varied from 400 mJ/cm^2 to 550 mJ/cm^2. Si islands with good size uniformity could be obtained at different laser fluences, and the diameters can be widely tuned from a 41.7 nm to a 147.1 nm depending on the laser fluence.

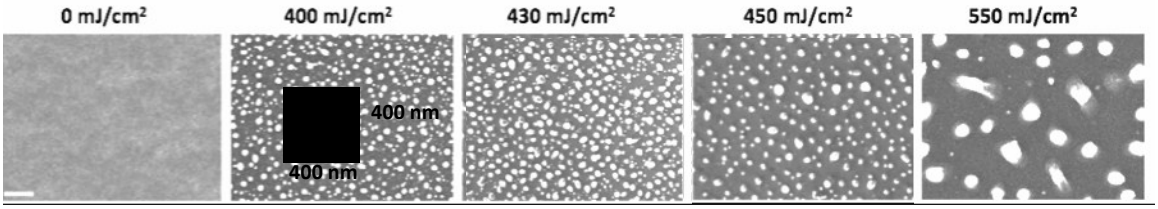

Figure 4. Calculating the density of the island structures

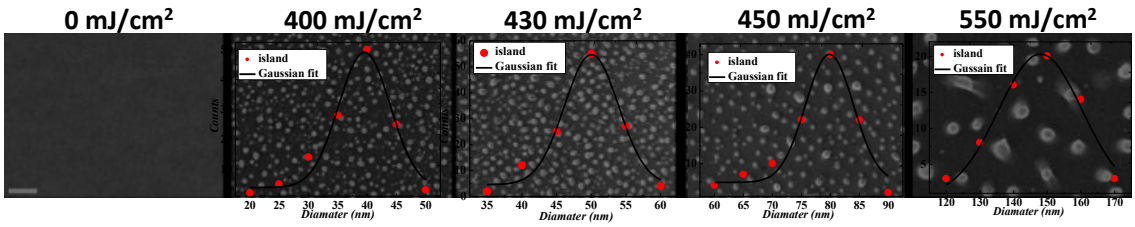

Figure 5. Calculating the of the mean diameters of island structures, in nanometers (nm)

3. Full Wave Numerical Simulations

All of the numerically calculated electric field distributions of the periodic nanostructures are obtained by FDTD simulation, and the hole parameters are based on the data from AFM images, as shown in figure 6. A background plane wave is traveling to Si surface nanohole arrays, and the periodic boundary condition is introduced into the numerically calculation. The dielectric constant of Si is set as 11.9. At last, we can get the local electric field distributions after numerically calculation.

3. Schematic illustration of mechanisms responsible for nanosecond laser-induced formation of surface ordered Si islands in patterned region.

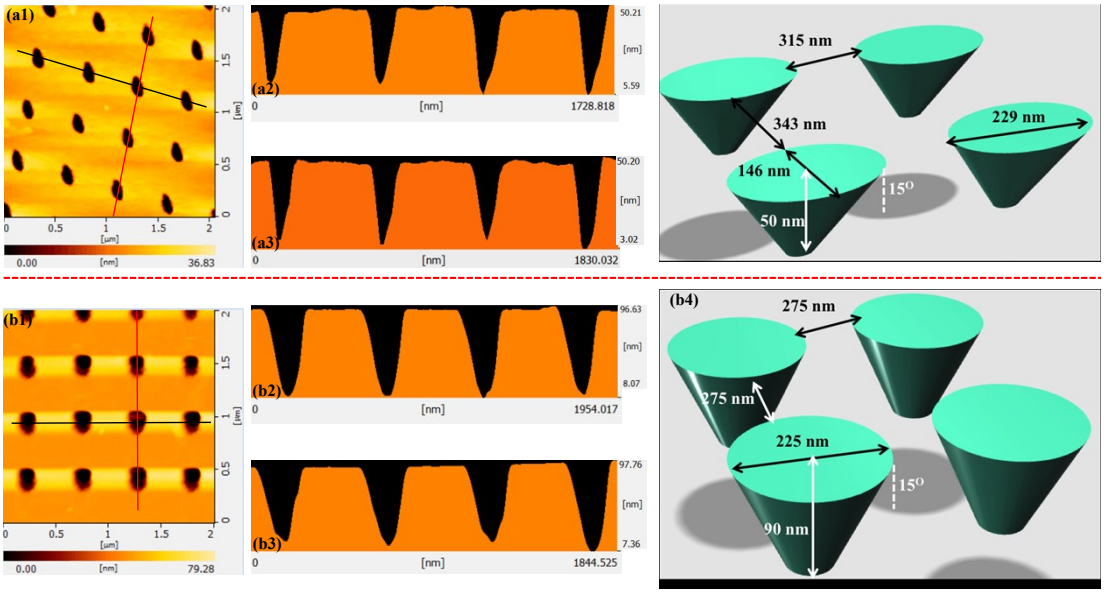

Figure 6. (a1, b1)，(a2, b3) and (a3, b3) are AFM images of height scans Si nanowell with different sizes.

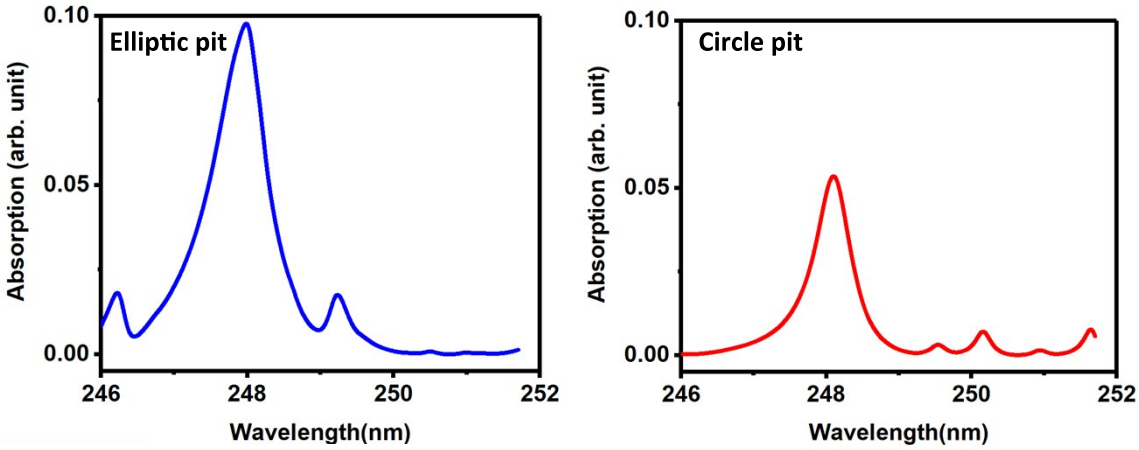

Figure 7. The absorption spectrum for the elliptic and circle pit

In this part, we mainly discuss the surface morphology evolutionary process vs laser fluence. In figure 7, for the untreated circle Si pit sub, the depth of each Si pit is about 88 nm, and after higher laser irradiation (550 mJ/cm^2), the patterned Si sub is replaced by disordered Si island structure, with the height of 20 nm and diameter of above 200 nm. Next, we modify the laser fluence, and symmetrical Si island structures can be formed on these surface electric hotspots by laser-induced directed dewetting processing. What more interesting is that the depth of the pit and the height of island also change with laser fluence, as shown in figure 7. Corresponding to untreated Si pit sub, the depth of the surface pits decrease after laser irradiation, besides, the depth of each pit also decrease with the laser fluence increasing. Oppositely, the height of the surface symmetrical Si islands increase with the increasing of laser fluence. Lastly, in order to give us a brief demonstration, we summary the tendency of depth of Si pit substrate and height of Si islands vs laser

fluence in figure 8. Basing on the above analyses, we conclude that, with the increasing of laser fluence, larger sized islands form near the edges are due to migration of adatoms from the inner wall of the pits and the nearby small size islands aggregation. In this case, the edge of pits can supply significant mass transfer and symmetrical islands are formed.

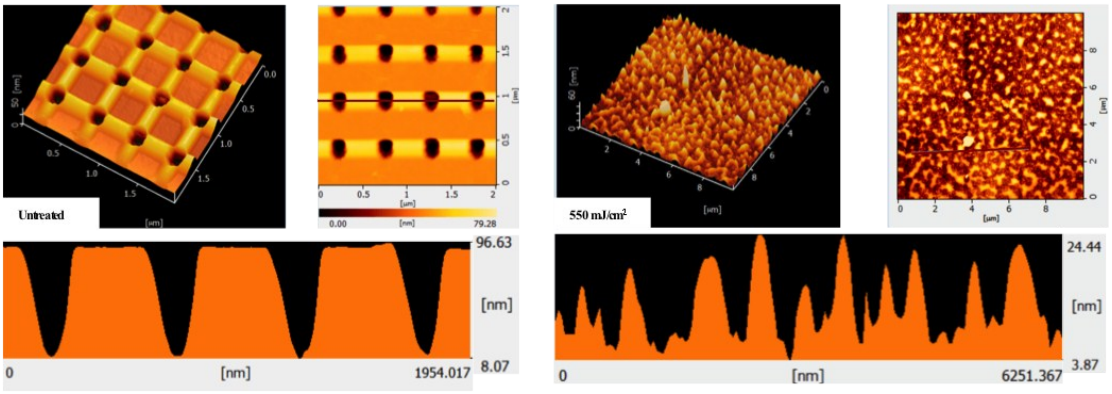

Figure 8. AFM images of surface morphology of Si pit substrate before and after higher laser irradiation.

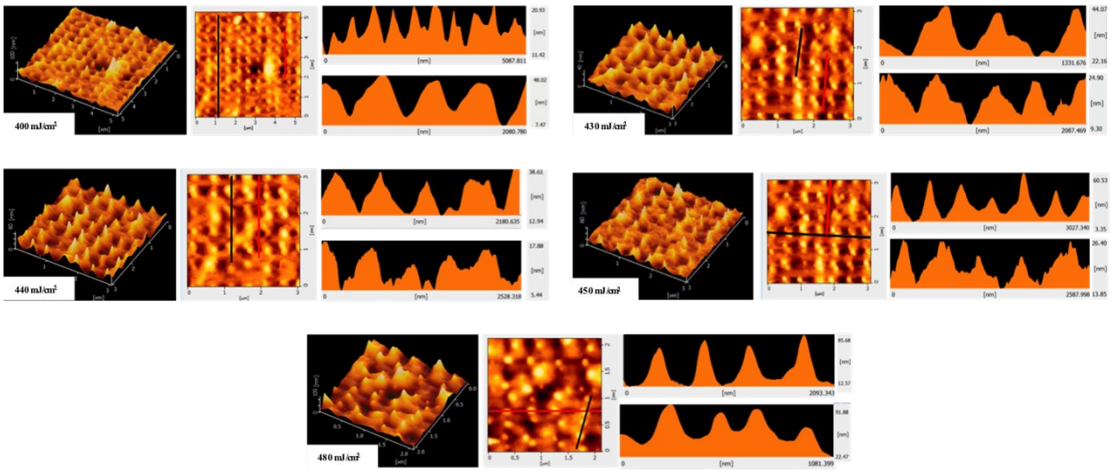

Figure 9. The tendency of depth of Si pit substrate and height of Si islands with the increasing laser fluence (from 400 mJ/cm^2 to 480 mJ/cm^2). In this image, basing on the AFM images, we give the detail information of the surface morphology with different laser fluence. The height of island and the depth of pit, in nanometers (nm) are (9.51, 40.55); (21.91, 15.6); (25.67, 12.44); (53.39, 12.55); (69.41, 3.7), respectively.

References:

(1) C. K.Ong, E.H. Sin, and H.S. Tan, *J. Opt. Soc. Am. B*, **1986**, 3(5), 812.
(2) Siti Rahmah Aid, Satoru Matsumoto, and Genshu Fuse, *Phys. Status Solidi A*. **2011**, 208(7), 1646–1651.

(3) C. M. Surko, A. L. Simons, D. H. Auston, J. A. Golovchenko, R. E. Slusher et al. *Appl. Phys. Lett.* **1979**, 34, 635.
(4) G. G. Bentini, M. Bianconi, and C. Summonte, *Appl. Phys. A*. **1988**, 45, 317-324.